THEORETICAL STUDY ON INFRARED THERMAL WAVE IMAGING DETECTION OF SEMICONDUCTOR SILICON WAFERS WITH MICRO-CRACK DEFECTS

by

Qing-Ju TANG[a,b*], Shuai-Shuai GAO[b], Yong-Jie LIU[b], Yun-Ze WANG[b], and Jing-Min DAI[a]

[a] School of Electrical Engineering and Automation, Harbin Institute of Technology, Harbin, China
[b] School of Mechanical Engineering, Heilongjiang University of Science and Technology, Harbin, China

Original scientific paper
https://doi.org/10.2298/TSCI2006011T

The semiconductor silicon wafer with micro-crack defects was detected using infrared thermal wave imaging technique. The 3-D thermal conduction model in semiconductor silicon wafer excited by linear frequency modulated continuous laser was established, and it was solved by finite element method. The results show the effectiveness of the proposed method for detecting micro-crack defects in semiconductor silicon wafers.

Key words: *infrared thermal wave imaging technique, micro-crack, semiconductor silicon wafer, infrared thermal imaging, linear frequency, finite element method*

Introduction

The semiconductor silicon wafer, as the main substrate material of integrated circuit (IC), has become the semiconductor material with the largest scale of production, the largest single crystal diameter and the most perfect production process. According to statistics, silicon devices account for more than 90% of all semiconductor devices sold in the world [1]. With the development of very large scale integration (VLSI) technology, the silicon wafer diameter increases and IC line-width decreases are put forward the higher requirements for the silicon wafer manufacturing process and surface qualities. From silicon ingot to silicon wafer, a series of mechanical and chemical processes such as cutting, grinding and polishing are needed. At present, self-rotating grinding is considered as the mainstream ultra-precision grinding method for processing large-size silicon wafers, and has been widely used. However, under the current technical conditions, a certain damage layer will be introduced in the process of ultra-precision grinding of silicon wafers. One of the important measures to optimize the quality of silicon wafers is to control the depth of the damage layer and improve the quality of the surface layer. The damage detection and evaluation of the surface layer of silicon wafers is an indispensable means in the process of studying the quality of silicon wafers processing [2]. The surface damage of silicon wafer can be divided into surface damage and sub-surface damage, including scratches, micro-cracks, crushing, orange peel and pits. The sub-surface damage includes amorphous

* Corresponding author, e-mail: tangqingju@126.com

layer, poly-crystalline layer, micro-cracks, dislocations, stacking faults, elastic distortion and residual stress [3]. These surface/subsurface damages in semiconductor wafer processing will affect the processing time and efficiency of subsequent polishing processes, and even threaten the yield, performance and service life of IC devices. Therefore, non-destructive testing, analysis and evaluation of surface/subsurface damage in semiconductor wafer production process is very necessary to achieve high efficiency, high precision and low damage processing of silicon wafer.

The commonly used destructive testing methods are preferred corrosion method, step-by-step corrosion method, section microscopy method and angle polishing method [4]. Infrared thermal non-destructive the testing (IR TNDT) is a new non-destructive testing method. Compared with conventional detection technology, it has many advantages [5], such as non-contact, large single detection area, easy to use in the field, safety, intuitive detection results and simple operation, so it has been more and more widely studied and applied. Laser has the characteristics of good monochrome, strong directivity, energy concentration and good coherence. It is easy to obtain uniform temperature field [6]. The photo-thermal effect mechanism and infrared thermal wave detection method of surface/subsurface damage of semiconductor silicon wafer excited by linear frequency modulation (LFM) laser are studied by combining the principle of LFM, laser excitation, infrared thermal wave detection and advanced signal processing algorithm.

The LFM is a new type of active infrared thermal wave non-destructive testing technology. It uses variable modulation frequency to excite semiconductor wafers, which makes up for some shortcomings of pulse method and phase-locked method, and can effectively detect micro-cracks on semiconductor wafers.

Numerical finite element method

Figure 1 shows the scheme of vertical finite crack inside a specimen. For the semiconductor silicon wafer structure with micro-crack damage, a 3-D thermal conduction model of semiconductor silicon wafer excited by LFM continuous laser is established.

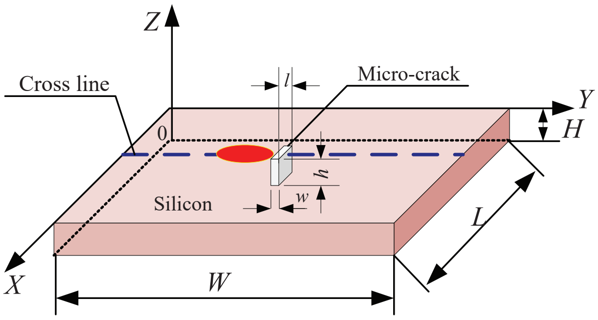

Figure 1. Scheme of vertical finite crack inside a sample

The heat conduction equation, initial conditions and boundary conditions can be expressed:

$$k_{xx}\frac{\partial^2 T}{\partial x^2}+k_{yy}\frac{\partial^2 T}{\partial y^2}+k_{zz}\frac{\partial^2 T}{\partial z^2}=\rho c\frac{\partial T}{\partial t} \tag{1}$$

$$T\left(x,y,z,t\right)\Big|_{t=0}=T\left(x,y,z,0\right)=T_{\mathrm{am}} \tag{2}$$

$$q\big|_{\mathrm{out}}=h\left[T_{\mathrm{am}}-T\left(x,y,z,t\right)\right]+\varepsilon\sigma\left[T_{\mathrm{am}}^4\right] \text{ and } q\left(t\right)\big|_{\Omega}=0 \tag{3a,b}$$

where k_{xx}, k_{yy}, and k_{zz} are thermal conductivity in three main directions, T – the temperature distribution, ρ – the density of the material, c – the specific heat capacity, $T(x,y,z,t)$ – the temperature of (x,y,z) at the moment of t, T_{am} – the ambient temperature, $T(x,y,z,0)$ – the temperature of (x,y,z) at $t=0$, which equals to T_{am}, $q|_{\mathrm{out}}$ – the heat flux of the bottom surface,

h – the convective heat transfer coefficient, ε – the emissivity of a surface, σ – the Stephen-Boltzmann constant, Ω – the micro-crack damage zone of the silicon wafer, and $q(t)$ – the heat flux of the top surface.

Suppose P is the laser power and ε is the power loss coefficient, then in a single pulse period, the heat flow loaded on the upper surface is given:

$$q(t) = q_{\mathrm{SC}} + q_{\mathrm{DC}}, \quad t \in [0, T] \tag{4}$$

where q_{SC} is static component of surface heat flow and q_{DC} is dynamic components of surface thermal flow.

The static and dynamic components can be expressed:

$$q_{\mathrm{SC}} = \frac{P\xi}{\pi\left(\frac{d}{2}\right)^2} \exp\left[-\frac{(x-x_1)^2 + (y-y_1)^2}{\left(\frac{d}{2}\right)^2}\right] \tag{5}$$

$$q_{\mathrm{DC}} = \frac{P\xi}{\pi\left(\frac{d}{2}\right)^2} \sin\left[2\pi\left(f_0 + \frac{f_e - f_0}{2T_s}t\right)t\right] \exp\left[-\frac{(x-x_1)^2 + (y-y_1)^2}{\left(\frac{d}{2}\right)^2}\right] \tag{6}$$

where P is the laser power, ξ – the power loss coefficient, d – the diameter of the laser spot, (x_1, y_1) – the Central co-ordinates of laser, f_0 – initial frequency of Chirp modulated signal, f_e – termination frequency of Chirp modulated signal, and T_s – scanning period of Chirp modulated signal.

Considering the preparation and service environment of the material, the material inside the crack is defined as air, and the thermal physical parameters of the material are shown in tab. 1. The geometrical parameters of the specimens used in finite element method (FEM) simulations are listed in tab. 2. In the laser thermal imaging detection system, parameters are selected as follows: laser power is 60 mW, time step is 0.1 second, chirp modulation parameter is 0.1-0.05-20, initial temperature is 293.15 K, spot diameter is 2 mm, specimen is $50 \times 50 \times 0.65$ mm^3. Figure 3 shows the scheme of vertical finite micro-crack inside a specimen. When the specimen surface is stimulated by LFM laser, it is affected by many factors. The main influencing factors are laser power, sampling frequency, convective heat transfer, laser beam diameter, chirp modulation parameters, spatial resolution and thermal imager noise.

Table 1. The thermal physical parameters

Material	Density [kgm^{-3}]	Specific heat capacity [Jkg^{-1}°C^{-1}]	Thermal conductivity coefficient [Wm^{-1}K^{-1}]
Silicon	2340	942.727	21.6
Air	1.29	1000	0.024

Results and discussion

Figure 2 shows the temperature distribution on the surface and across line at 3.5 seconds.

From fig. 2(a), it can be seen that micro-cracks hinder the heat transfer in the specimen. Micro-cracks divide the heat transfer area near the micro-crack into two parts, the heat source

Table 2. Geometrical parameters of micro-cracks in specimens

No.	l [mm]	w [mm]	h [mm]
Crack 1	10	0.02	0.1
Crack 2	10	0.02	0.2
Crack 3	10	0.02	0.3
Crack 4	10	0.02	0.4
Crack 5	10	0.01	0.2
Crack 6	10	0.03	0.2
Crack 7	10	0.04	0.2
Crack 8	4	0.02	0.2
Crack 9	13	0.02	0.2
Crack 10	16	0.02	0.2

area and the non-heat source area, respectively. The temperature of the heat source area is higher than that of the non-crack area at the same location, and the temperature of the non-heat source area is lower than that of the non-crack area at the same location. Surface temperature distribution jumps at the micro-crack, which is affected by micro-crack width, micro-crack depth and other factors. For a 10-micron micro-crack, the center of the micro-crack near the laser spot is 295.629 K, and the temperature of the other side of the micro-crack is 296.030 K. The difference between them is 0.401 K. It is shown that under these detection parameters, the micro-crack of 10 micron can be identified effectively by using infrared thermal imager with minimum identification temperature difference less than 0.401 K in theory. Figure 2(b) shows the surface temperature abrupt jump between the two sides of crack. From fig. 2(b), it can be seen that the temperature curve is smooth at the crack-free place, and the temperature changes steadily. At the micro-crack place, the temperature curve has a sudden change and the temperature jumps.

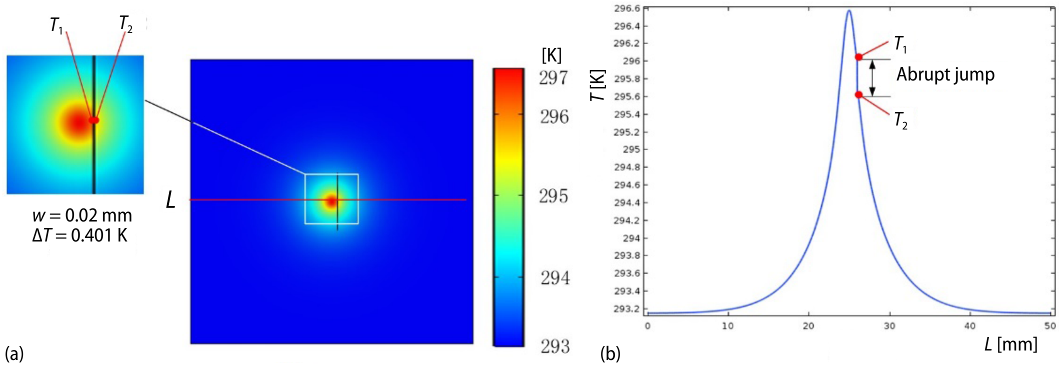

Figure 2. Temperature distribution on specimen surface and across line at 3.5 seconds; (a) surface temperature distribution of the specimen and (b) surface temperature abrupt jump between the two sides of crack

Effect of crack width on surface temperature difference of micro-cracks

Figure 3 shows that when the length of the micro-crack is 10 mm, the depth of the micro-crack is 0.02 mm, and the width of the micro-crack is 0.01 mm, 0.02 mm, 0.03 mm, and 0.04 mm, respectively, the curve has a process of increasing and decreasing. Each curve has three peaks of temperature difference. By comparing the curves with different widths, it can be seen that the curve with the crack width of 0.04 mm at the top, followed by the curves with the width of 0.03 mm, 0.02 mm, and 0.01 mm in turn, indicating that the wider the micro-crack width, the greater the temperature difference between the two sides of the micro-crack, the easier to be detected. With the increase of micro-crack widths, the maximum temperature difference curves on both sides of the micro-crack show an upward trend.

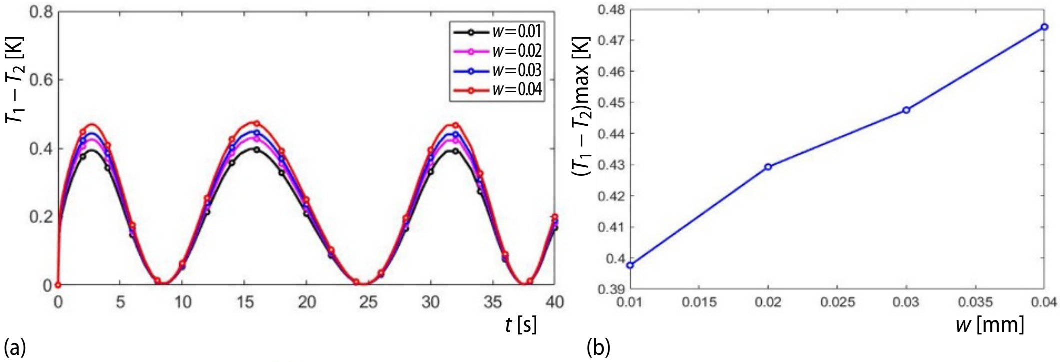

Figure 3. Temperature difference curves on both sides of different micro-crack widths; (a) temperature difference curves and (b) maximum temperature difference curve

Effect of depth on surface temperature difference of micro-cracks

Figure 4 shows that when the length of micro-crack is 10 mm, the width of micro-crack is 0.02 mm, and the depth of micro-crack is 0.1 mm, 0.2 mm, 0.3 mm, and 0.4 mm, respectively, the curves increase and decrease. Comparing the curves of different depths, it can be seen that the curve of crack depth is 0.4 mm at the top, and the curve of crack depth is 0.3 mm, 0.2 mm, and 0.1 mm at the bottom. The greater the temperature difference, the easier to be detected. With the increase of micro-crack depth, the maximum temperature difference curves at both sides of the micro-crack show an upward trend.

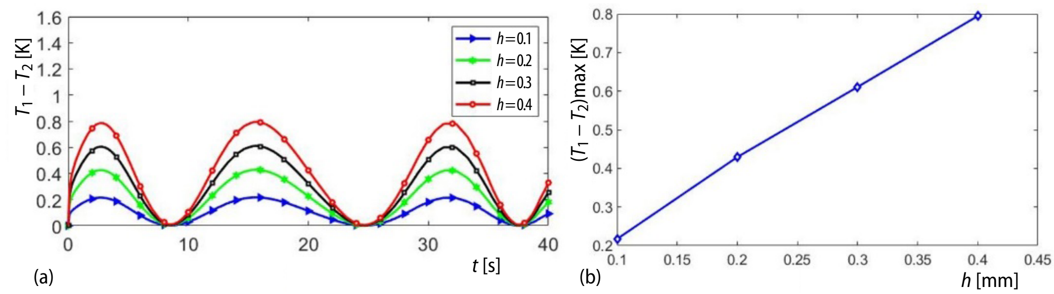

Figure 4. Temperature difference curves on both sides of different micro-crack depths; (a) temperature difference curves and (b) maximum temperature difference curve

Effect of laser power on surface temperature difference of micro-cracks

Figure 5 shows the influence of different power on the temperature difference between the two sides of the micro-crack. It can be seen that the temperature difference between the two sides of the micro-crack with 200 mW power is the largest, followed by 150 mW, 100 mW, and 60 mW. With the increase of the laser power, the maximum temperature difference on both sides of the micro-crack increases.

Effect of scanning period on surface temperature difference of micro-cracks

Figure 6 shows the curve of temperature difference on both sides of the micro-crack with different scanning period.

It can be seen that the four curves in the figure almost coincide before 8 seconds. Different scanning period will lead to changes in the applied heat flow. The temperature differ-

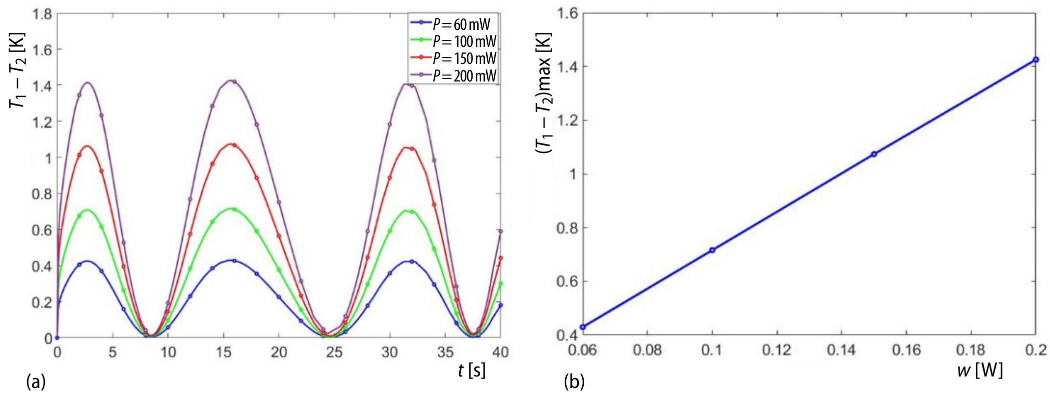

Figure 5. Effect of different power on temperature difference on both sides of the micro-crack; (a) temperature difference curves and (b) maximum temperature difference curve

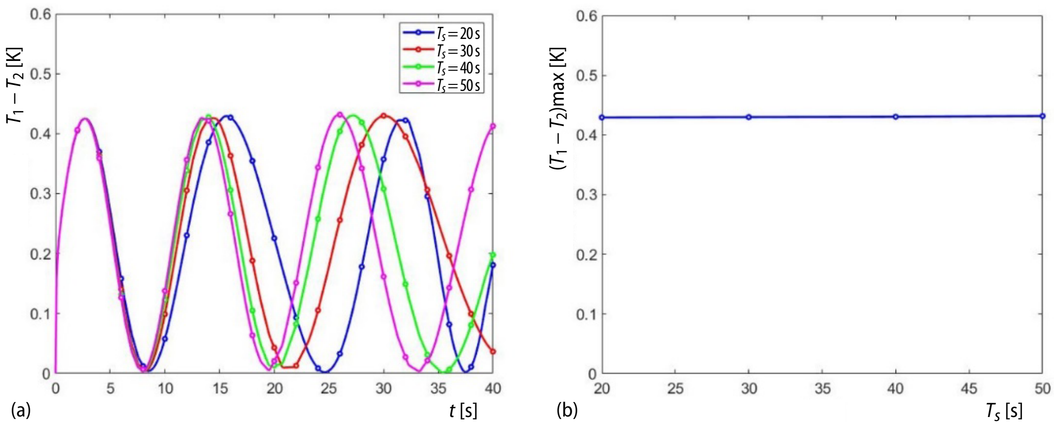

Figure 6. Curve of temperature difference on both sides of the micro-crack with different scanning period; (a) temperature difference curves and (b) maximum temperature difference curve

ence varies with the change of power. The difference increases gradually from 10 seconds and can be clearly distinguished. It shows that the change of the maximum temperature difference in the scanning period has no effect. With the increase of scanning period, the variation curves do not change much, which shows that the scanning period have little effect on the maximum temperature difference curves of the two sides of the micro-crack.

Conclusion

In this work, the semiconductor silicon wafer with micro-crack defects excited by linear frequency modulated continuous laser was detected using infrared thermal wave imaging technique. The 3-D thermal conduction model in semiconductor silicon was established and solved by FEM. Results show that a micro-crack with the width of 10 μm can be detected theoretically. With the increasing of the micro-crack's depth and width, the temperature difference between the two sides of the micro-cracks increases. Without causing secondary damage to semiconductor silicon wafers and within the permissible range of detection system, increasing laser power can better identify micro-crack defects, while scanning period has little effect on that.

Acknowledgment

This study is sponsored by National Natural Science Foundation of China (Grant No. 51775175), Special Financial Grant from the China Postdoctoral Science Foundation (Grant No. 2016T90278), and China Postdoctoral Science Foundation the Fifty-Eighth Batch (Grant No. 2015M80258), and Heilongjiang Postdoctoral Fund to Pursue Scientific Research (Grant No. LBH-Z15091).

References

[1] Canale, J. E., *et al*., Glass Wafers for Semiconductors Fabrication Processes and Methods of Making Same, *Life Sciences*, *9* (2015), pp, 989-1001
[2] Guo, X., *et al.*, Molecular Dynamics Study on the Thickness of Damage Layer in Multiple Grinding of Monocrystalline Silicon, *Materials Science in Semiconductor Processing*, *51* (2016), Aug., pp, 15-19
[3] Liu, T., *et al.*, Subsurface Crack Damage in Silicon Wafers Induced ny Resin Bonded Diamond Wire Sawing, *Materials Science in Semiconductor Processing*, *57* (2017), C, pp, 147-156
[4] Woo, T. K., *et al.*, Three-Dimensional Dual-Porous Structure Developed by Preferential/Stain Etching on Grind-Damaged (001) Si: Formation and Optical Properties, *Journal of the Electrochemical Society, 159* (2012), 1, pp, P1-P7
[5] Abreu, L. A. S., *et al*., Thermography Detection of Contact Failures in Double Layered Materials using the Reciprocity Functional Approach, *Applied Thermal Engineering, 100* (2016), May, pp, 1173-1178
[6] Kime, L., *et al.*, High-Flux Monochromatic Ion and Electron Beams Based on Laser-Cooled Atoms, *Physical Review A*, *88* (2013), Sept., 033424

Paper submitted: June 1, 2020
Paper revised: July 1, 2020
Paper accepted: July 10, 2020